FINAL REPORT
ON THE INTEREST PROGRAMME

Soft photon study in hadron and nuclear interactions

Supervisor:
Prof Elena Kokoulina

Student:
Murashka Stanislau
Medical physics,

International Sakharov Environmental Institute
of Belarusian State University

Participation period:
June 13 - July 22, Wave 7

Introduction

To date, there is a significant discrepancy between experimental data and quantum electrodynamics calculations for photons with energies below 50 MeV, which is formed by hadron and nuclear interactions [1].

Up to now the nature of these photons remains enigmatic. Apparently, they are formed in the region of non perturbative quantum chromodynamics and physicists build phenomenological models. The most successful model is based on the hypothesis of the cold quark-gluon plasma (QGP) formation. This model implies the formation of a quark-gluon system which consists of a few quarks, antiquarks and gluons. These partons are encountering each other and reradiate photons because they do not have enough energy to produce hadrons [1].

The NICA accelerator complex, which is currently under construction, will make it possible to conduct studies of pp, pA and AA interactions at energies up to 25 GeV in the future. Thus, at NICA it is possible to further study the yield of photons with energies of tens of MeV [1].

Project goals

- Acquaintance with Geant4 Monte Carlo simulation package and ROOT data analysis program.
- Data taking and data processing for geant4 simulations.
- Study of the operation of electromagnetic calorimeters of homogeneous and sampling types.

Radiation interaction with matter

High-energy photons and electrons can interact with media producing secondary particles which leads to a shower development. For photons with energies less than 50 MeV, the shower is mainly an electromagnetic cascade consisting of photons and electrons (positrons) [2]. The formation of charged particles by photons occurs in the following processes: photoelectric absorption, Compton scattering and electron-positron production in the fields of the nucleus and of the atomic electrons.

The main interactions of charged particles with matter are ionisation and excitation of absorber material, and for relativistic electrons – bremsstrahlung. Energy measurements in ionization chambers are based on secondary electrons wich formed during ionization, and the use of scintillation detectors is based on the emission of visible light during relaxation.

The high-enegy electrons predominantly lose energy by bremsstrahlung, and high-energy photons by pair production. The radiation losses of electrons can

be described by radiation length. In a monatomic material, the mean distance at which the electron energy decreases by a factor of $\boldsymbol{e}$ can be approximately calculated by the formula 1 [2].

$$X_0 \approx \frac{716.4 \cdot A \left[\mathrm{g\,mol^{-1}}\right]}{Z\left(Z+1\right)\ln\left(287/\sqrt{Z}\right)} \quad \mathrm{g\,cm^{-2}}. \tag{1}$$

The effective values for Z and A of mixtures and compounds can be calculated for A by

$$\begin{aligned} A_{eff} &= \sum_{i=1}^{N} f_i A_i \\ Z_{eff}\left(Z_{eff}+1\right) &= \sum_{i=1}^{N} f_i Z_i \left(Z_i+1\right) \end{aligned} \tag{2}$$

where f_i are the mass fractions of the components with atomic weight A_i and charge numbers Z_i [2]. For molecules, f_i is equal to

$$f_i = \frac{A_i \nu_i}{\sum\limits_{k=1}^{N} A_k \nu_k} \quad , \tag{3}$$

where ν are numbers of A_i atoms in the molecule.

To obtain the radiation length expressed in cm, we have to divide formula 1 by the density ρ of the compound.

Using the value X_0, it is also possible to obtain the probability of the formation of an electron-positron pair by high-energy photons [2]

$$\frac{\mathrm{d}\omega}{\mathrm{d}x} \approx \frac{1}{\lambda_{prod}} \exp\left(\frac{-x}{\lambda_{prod}}\right) \quad , \qquad \lambda_{prod} \approx \frac{9}{7} X_0 \quad . \tag{4}$$

In the formula (4) λ_{prod} represents mean free path for pair production.

By simplifying the processes occurring in the electromagnetic cascade, the following patterns can be obtained [2]:

- To absorb most of the energy of the incident photon the total calorimeter thickness should be more than 10-15 X_0.
- The position of the shower maximum increases slowly with energy. Hence, the thickness of the calorimeter should increase as the logarithm.
- The energy leakage is caused mostly by soft photons escaping the calorimeter at the sides (lateral leakage) or at the back (rearleakage).

The angular distribution of the pair production from primary photons is very narrow. And the lateral width of an electromagnetic cascade is mostly determined by multiple scattering and can be characterised by the Molière radius

$$R_M = \frac{21\,\mathrm{MeV}}{E_C} X_0 \quad \left\{\mathrm{g\,cm^{-2}}\right\} \quad . \tag{5}$$

where E_C – critical energy, which describe the energy, when processes ionization and bremsstrahlung for electrons lead to equal energy losses. On average, a cylinder with a Molière radius contains about 90% of the energy of an electromagnetic cascade [2, 3].

For for solids and liquids , the critical energy can be approximately calculated using the following formula [3]

$$E_C = \frac{610\,\mathrm{MeV}}{Z + 1.24} \quad . \tag{6}$$

Electromagnetic calorimeter

Electromagnetic calorimeters are primarily targeting electrons and photons but normally will also produce signals for other types of particles. The key task for calorimeters is to transmit signals generated by energy deposits inside the detector volume to the outside, which determines the overall design, the choice of reading geometry and detector materials. The requirements for detector depth in units of X_0, often competing with space constraints, lead to a preference for materials with higher density. Goals regarding energy resolution and other performance parameters affect the choice of the active detector material, and in the case of sampling calorimeters, also the choice of the passive absorber material and geometric structure [2, 3].

Homogeneous calorimeters

Homogeneous calorimeters are constructed from a material combining the properties of an absorber and a detector. It means that practically the total volume of the calorimeter is sensitive to the deposited energy. This type of calorimeters are used in particular when excellent energy resolution is required [3].

Typical active materials are scintillating crystals or glasses making use of the Cherenkov effect for signal generation. The yield of Cherenkov photons is lower by approximately another order of magnitude, making this a key limiting factor for the energy resolution in Cherenkov-based calorimeters. In addition to crystal- and glass-based detectors, also the deep UV scintillation of cryogenic liquids such as liquid xenon and liquid krypton, as well as Cherenkov light emission in water, is used for calorimetric measurements. Due to the properties of hadronic showers, homogeneous calorimeters are typically only well suited for the detection

of electromagnetic showers, in terms of both required overall detector depth and achievable energy resolution [3].

Sampling calorimeters

A sampling calorimeter is a calorimeter designed as an array of thin sensitive detector separated by absorber and only a sample of the energy deposition is measured. There are at least 2 types of calorimeters: "spaghetti", in which the scintillator is directed along the direction of the detector, and "sandwich", which has a sandwich structure [3].

Since the passive material of sampling calorimeters can be selected with a high-density absorber, they have a smaller size compared to homogeneous calorimeters. They are usually also significantly lower in cost per instrumented volume than homogeneous calorimeters, with details depending on the choice of active and passive materials. Sampling calorimeters typically do not reach the same level of energy resolution as homogeneous [3].

Detector Construction

Pure Cesium iodide crystal

Pure CsI is an Unactivated Fast Inorganics scintillator with a Specific gravity of $4.51\,\mathrm{g\,cm^{-3}}$ and absolute light yield of the fast component equal to 2000 Photons per MeV. Much of this light shows a mixture of a mixture of fast components with an effective decay time of about 10 ns that appears in a peak around 305 nm 305 nm in the ultraviolet region of the spectrum. A broader emission band in the visible range of 350 to 600 nm that has a much longer decay time of up to several microseconds is also often observed [4].

The radiation length of the CsI is 1.860 cm, and the Molière radius is 3.531 cm [5]. 1.5" radius ($1.08 \cdot R_M$) x 6" long ($8.19 \cdot X_0$) is a typical crystal size produced by commercial companies [6].

In this work, 2 CsI detectors were modeled:

1. typical 1.5" radius x 6" long crystal.

2. Parallelepiped crystal with a size of 10 cm x 10 cm x 30.48 cm.

"Sandwich" calorimeter with plastic scintillator and lead absorber

For this detector, a sheet of lead with a thickness of 1 mm and plates of BC412 scintillation plastic with a thickness of 3 mm were selected. BC412 (Saint-Gobain Crystals classification) has a 3.3 ns decay time and 60% light yield compared to anthracene, which is approximately 9900 ph. per MeV [4]. The density of this scintillation plastic is $1.032\,\mathrm{g\,cm^{-3}}$ and the H/C ratio is 1.104 [7].

Table 1: Properties of the component elements of the BC412

Elements	Z	A ($g\,mol^{-1}$)	N. Atoms per cc (x10^{22}) [7]	f_i (%)
H	1	1.00794	5.23	8.47
C	6	12.0107	4.74	91.53

The calorimeter consists of 57 absorber sheets and 56 scintillator plates. The thickness of 56 mm is about 10[8] radiation lengths of lead. The total size is 20 cm x 20 cm x 22.5 cm.

Geant4 Simulations

Run settings

Simulations were performed in the Geant4 package version 10.7.3 For interaction computations, the standard library of electromagnetic processes was used in Geant4. ParticleGun was set to single-photon irradiation, with a gamma-ray energy of 50 MeV.

The source of isotropic radiation had a point geometry and was located at a distance of 1 meter from the front of the electromagnetic calorimeter. At the same time, the center of the detector and the source of γ-rays were located on the coordinate axis Oz. The primary irradiation was collimated along the azimuthal angle using a modified code from **G4RandomDirection.hh**.

Simulations were carried out for five irradiation geometries:

1. Irradiation of the entire front surface of the detector.

2-5. Cones formed by spherical sectors of irradiation and the front surface of the calorimeter, with base diameters equal to 1, 1/2, 1/4 and 1/8 of the width (diameter) of the calorimeter.

For the first three geometries listed above, the number of events was 160000, for 1/4 and 1/8 geometries – 90000. The total energy absorbed by the scintillator was recorded in the corresponding root file.

Simulation results

After the calculations, the distribution was normalized for non-zero values of absorbed energy in scintillators. The total absorbed energy in homogeneous electromagnetic calorimeters is presented in Figures 1 and 2. Figure 3 shows the energy spectrum in the scintillation plastic for the sandwich.

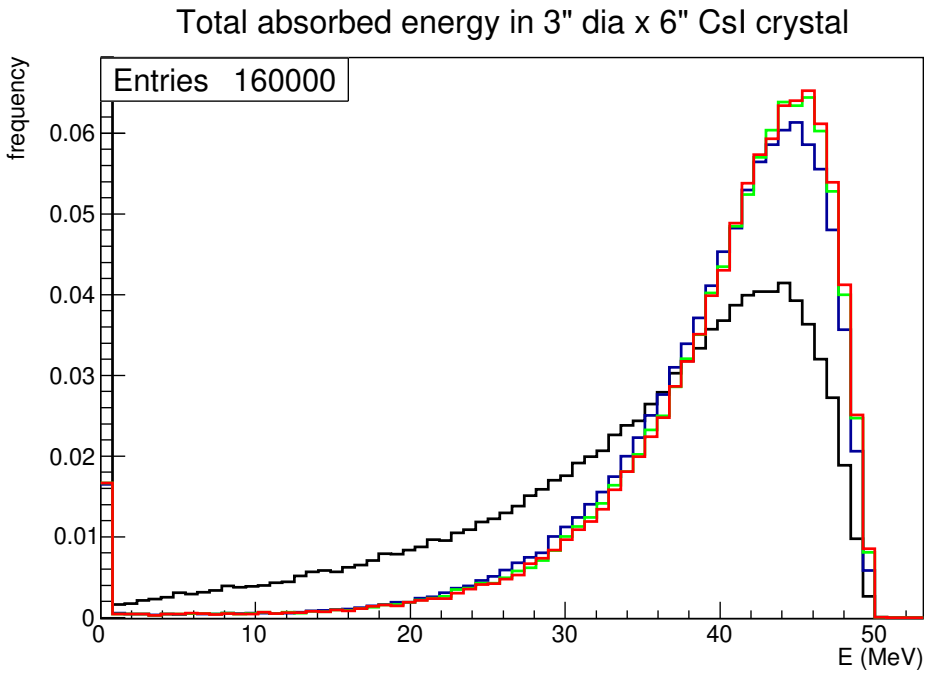

Figure 1: The spectrum of the total absorbed energy in the crystal for 50 MeV photons. The black color corresponds to the irradiation of the entire front surface of the detector. Blue, green and red correspond to 1/2, 1/4 and 1/8 diameter geometries of irradiation, respectively.

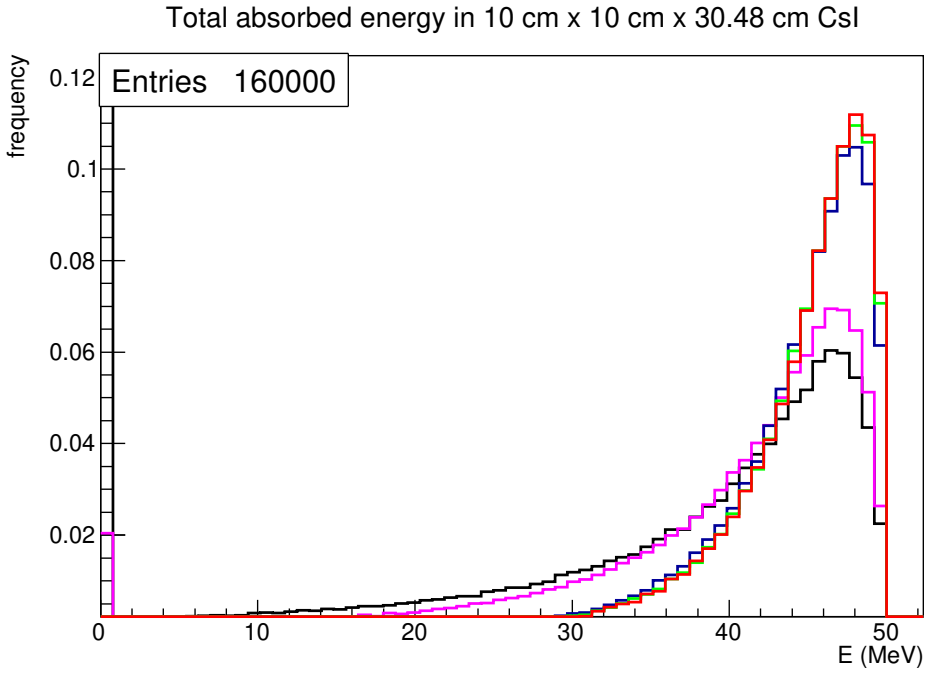

Figure 2: The spectrum of the total absorbed energy in the crystal for 50 MeV photons. Black color corresponds to the irradiation of the entire front surface. Purple, blue, green and red correspond to 1, 1/2, 1/4 and 1/8 width geometries of irradiation, respectively.

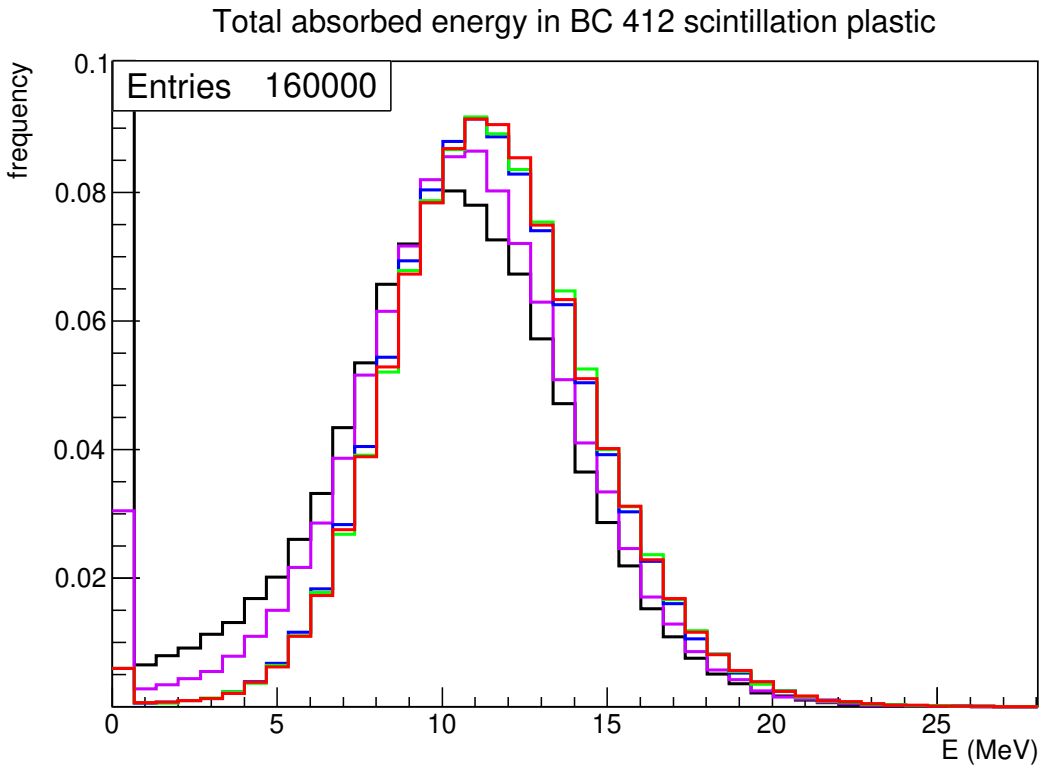

Figure 3: The spectrum of the total absorbed energy in the crystal for 50 MeV photons. Black color corresponds to the irradiation of the entire front surface. Purple, blue, green and red correspond to 1, 1/2, 1/4 and 1/8 width geometries of irradiation, respectively.

Conclusions

Monte Carlo modeling methods allow one to evaluate the interactions of ionizing radiation with matter by numerical methods. This allows programs such as Geant 4 to be used to develop detector designs and signal reconstruction algorithms.

The description of the processes that occur in Geant4 simulations is based on models. Thus, comparison of the results of calculations with experimental data makes it possible to assess the adequacy of these models and the correspondence of the theories on which these models are based to reality.

In this study were constructed two different types of calorimeteres: a homogeneous one based on a pure CsI crystal and a sampling calorimeter having as a detector material BC412 scintillation plastic and Pb as an absorber. It should be noted that this work didn't consider questions concerning the device of the electronic part of the detector, algorithms for signal reconstruction and degradation of the calorimeter caused by radiation damage.

References

1. Kokoulina, E., Barlykov, N., Dudin, V., Dunin, V., Kutov, A., Nikitin, V., Riadovikov, V. and Shulyakovsky, R., (2020). Study of soft photon yield in pp and AA interactions at JINR. *EPJ Web of Conferences*, 235, p.03003.

2. Grupen, C., & Shwartz, B. (2008). *Particle Detectors* (2nd ed.). Cambridge University Press.

3. Fleck, I., Titov, M., Grupen, C., & Buvat, I. (2021). *Handbook of Particle Detection and Imaging* (2nd ed.). Springer.

4. Knoll, G. F. (2010). *Radiation Detection and Measurement* (4th ed.). Wiley.

5. Atomic and nuclear properties of cesium iodide (CsI). (n.d). Particle Data Group Retrieved July 01, 2022, from https://pdg.lbl.gov/2022/AtomicNuclearProperties/HTML/cesium_iodide_CsI.html.

6. *CsI Cesium Iodide*. (n.d.). Saint-Gobain Crystals. Retrieved June 29, 2022, from https://www.crystals.saint-gobain.com/radiation-detection-scintillators/crystal-scintillators/csi-cesium-iodide.

7. *BC-400, BC-404, BC-408, BC-412, BC-416 General Purpose*. (n.d.). Saint-Gobain Crystals. Retrieved June 29, 2022, from https://www.crystals.saint-gobain.com/radiation-detection-scintillators/plastic-scintillators/bc-400-bc-404-bc-408-bc-412-bc-416.

8. Atomic and nuclear properties of lead (Pb). (n.d). Particle Data Group Retrieved July 01, 2022, from https://pdg.lbl.gov/2022/AtomicNuclearProperties/HTML/lead_Pb.html.